

Strong electron-phonon and band structure effects in the optical properties of high pressure metallic hydrogen

Miguel Borinaga,^{1,2} Julen Ibañez-Azpiroz,³ Aitor Bergara,^{1,2,4} and Ion Errea^{2,5}

¹*Centro de Física de Materiales CFM, CSIC-UPV/EHU,*

Paseo Manuel de Lardizabal 5, 20018 Donostia/San Sebastián, Basque Country, Spain

²*Donostia International Physics Center (DIPC), Manuel Lardizabal pasealekua 4,*

20018 Donostia/San Sebastián, Basque Country, Spain

³*Peter Grünberg Institute and Institute for Advanced Simulation,*

Forschungszentrum Jülich & JARA, D-52425 Jülich, Germany

⁴*Departamento de Física de la Materia Condensada,*

University of the Basque Country (UPV/EHU), 48080 Bilbao, Basque Country, Spain

⁵*Fisika Aplikatua 1 Saila, Bilboko Ingeniaritza Eskola, University of the Basque Country (UPV/EHU),*

Rafael Moreno "Pitxitri" Pasealekua 3, 48013 Bilbao, Basque Country, Spain

(Dated: March 12, 2022)

Characterization of the first ever laboratory produced metallic hydrogen sample relies on measurements of optical spectra. Here we present first-principles calculations of the reflectivity of hydrogen between 400 and 600 GPa in the $I4_1/amd$ crystal structure, the one predicted at these pressures, based on both time-dependent density functional and Eliashberg theories, thus, covering the optical properties from the infrared to the ultraviolet regimes. Our results show that atomic hydrogen displays an interband plasmon at around 6 eV that abruptly suppresses the reflectivity, while the large superconducting gap energy yields a sharp decrease of the reflectivity in the infrared region approximately at 120 meV. The experimentally estimated electronic scattering rates in the 0.7-3 eV range are in agreement with our theoretical estimations, which show that the huge electron-phonon interaction of the system dominates the electronic scattering in this energy range. The remarkable features in the optical spectra predicted here encourage to extend the existing optical measurements to the infrared and ultraviolet regions.

Wigner and Huntington predicted back in 1935 that at high pressure hydrogen molecules would dissociate yielding a metallic compound similar to the alkalis¹. Metallic hydrogen is expected to be a wonder material as it may superconduct at ambient temperature²⁻⁸ and provide a very powerful rocket fuel⁹. Despite a huge experimental effort in the last years has characterized the phase diagram of hydrogen up to very high pressures¹⁰⁻²¹, metallic hydrogen has remained elusive. Remarkably, however, the long standing quest might have come to an end as, early this year, Dias and Silvera reported the first ever laboratory-produced sample of metallic hydrogen²².

Metallic hydrogen was claimed to have been observed as the sample became reflective above 495 GPa²². The claim remains controversial as doubts on the pressure calibration have been raised and a semiconducting sample may also be reflective²³⁻²⁶. Moreover, raw reflectance data in Ref. [22] shows a sharp decrease for photon energies larger than 2 eV whose origin is not totally understood even though it was first attributed to absorption of diamond²⁷. In any case, the claim of having produced metallic hydrogen comes after previous works in which the first signals of its existence were present or close to appear^{21,28}. Thus, reproducibility of the experiment and exhaustive characterization of the system clearly are the next challenge. Characterizing hydrogen under pressure is extremely difficult due to the limitations imposed on conventional techniques. Unavailability of neutron scattering and x-ray diffraction experiments for extremely high-pressure hydrogen samples in

Diamond-Anvil-Cells makes the use of alternative techniques imperative. Many of the already known solid hydrogen phases have been characterized by comparing Raman scattering and infrared (IR) absorption data to theoretical calculations^{10,15-18,21,29}. Comparing optical reflectance spectra to theoretical estimations is indeed another option^{22,30}.

In this letter we report an exhaustive characterization of the optical response properties from the IR to the extreme ultraviolet (UV) of metallic hydrogen between 400 and 600 GPa in the atomic $I4_1/amd$ phase, the structure predicted for hydrogen at these pressures^{31,32}. Our fully first-principles analysis based on density-functional theory (DFT) sheds light into the regime measured by Dias and Silvera²², from 0.75 to 3 eV photon energies, showing that in this range the electronic relaxation time is dominated by the huge electron-phonon interaction. Besides, our calculations predict a complex reflectance spectrum not expected *a priori* for a free-electron-like alkali metal. On one hand, our calculations reveal a sharp onset of the optical conductivity in the IR region induced by the very large superconducting gap of atomic hydrogen⁷. This suggests that reflectivity measurements in the IR region at temperatures below the superconducting critical temperature T_c , predicted to be of 300 K⁷, might be used to measure optically T_c and the superconducting gap as it occurs, for instance, in cuprates³³, alkali-metal-doped fullerenes³⁴, and the recently discovered³⁵ record superconductor H_3S ³⁶. On the other extreme, the UV regime exhibits a pronounced loss of reflectance due to the pres-

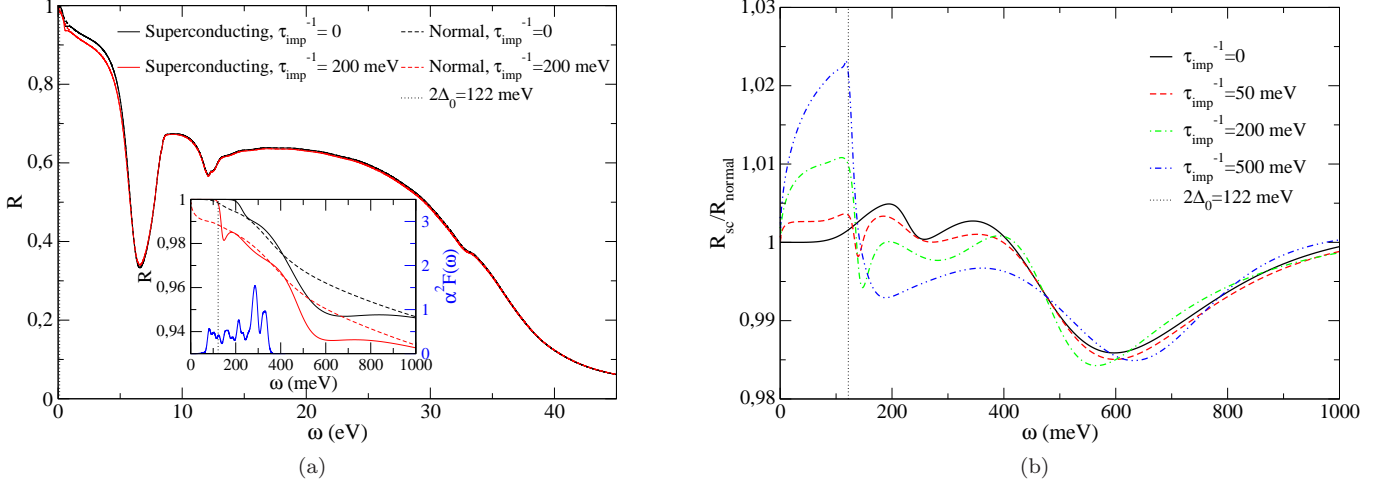


Figure 1. (a) Reflectivity of I4₁/amd hydrogen in vacuum at 50 K and 500 GPa for different impurity scattering rates both in the normal and superconducting states. The inset shows the same curves at the low energy regime along with the electron-phonon spectral function $\alpha^2 F(\omega)$. (b) Ratio between superconducting and normal state reflectance of I4₁/amd hydrogen in vacuum at 50 K and 500 GPa for different impurity scattering rates.

ence of a non-free-electron-like interband plasmon. Our results therefore provide clear means of characterizing metallic hydrogen via these singular features, strongly encouraging the extension of experimental optical measurements²² to broader regimes.

The central quantity addressed in this work is the frequency dependent reflectivity, which for normal incident light in a medium with refractive index n can be written as

$$R(\omega) = \left| \frac{\sqrt{\varepsilon(\omega)} - n}{\sqrt{\varepsilon(\omega)} + n} \right|^2. \quad (1)$$

We have calculated the relative dielectric function $\varepsilon(\omega)$ by combining time-dependent DFT^{37–39} (TDDFT), which realistically incorporates the actual electronic structure into the dielectric function, and isotropic Migdal-Eliashberg (ME) equations, which take into account how an excited electron can decay due to the electron-phonon interaction (see the Supplementary Material for a more detailed description of the methods and the calculation procedure). ME equations are solved with different τ_{imp}^{-1} impurity scattering rates. This enables us to properly account for the optical features of metallic and presumably superconducting hydrogen not only in the visible and UV, but also in the IR, which could be strongly affected due to the presence of the superconducting gap Δ_0 ^{33,34,36}. All the calculations presented in this letter are performed at 500 GPa, where metallic hydrogen is predicted to adopt the I4₁/amd crystal structure^{31,32}. Calculations performed at 400 and 600 GPa presented in the Supplementary Material show a very weak pressure dependence of the reflectivity as only minor quantitative but not qualitative differences are observed. Thus, the analysis presented here holds at higher and lower pressures.

In Fig. 1a we show the calculated reflectivity of I4₁/amd hydrogen in vacuum ($n = 1$ in eq. (1)) in the low temperature limit (50 K) at 500 GPa, for both the normal and superconducting states. We find two different regimes for the optical spectra: the IR regime ($\omega < 1$ eV), where the effects related to scattering with phonons and impurities dominate; and the visible and UV regime ($\omega > 1$ eV) where electronic band structure effects start to play a role.

The inset in Fig. 1a shows the low temperature limit of the reflectivity at 500 GPa for IR radiation. Clean hydrogen ($\tau_{imp}^{-1} = 0$) in the normal state (which can be obtained by setting $\Delta_0 = 0$ in ME equations) reflects all the incoming light until phonons start contributing substantially to $\alpha^2 F(\omega)$ above ~ 100 meV. When impurity scattering is taken into account reflectivity decreases from 1 right from the beginning, reaching a small plateau (~ 0.99 for $\tau_{imp}^{-1} = 200$ meV) until scattering with phonons starts to be relevant. In the superconducting state the reflectivity is equal to unity below $2\Delta_0 = 122$ meV even when impurity scattering is taken into account, as that is the amount of energy required to break a Cooper pair and make electrons contribute to the optical conductivity. This can be clearly seen in Fig. 2b, where $\text{Im } \varepsilon$ is strictly zero below $2\Delta_0$ (except the zero frequency contribution coming from the DC conductivity of the Cooper pairs) abruptly increasing at larger energies. While for $\tau_{imp}^{-1} = 200$ meV the gap is clearly observable due to the sudden decrease of R , it is not the same for the clean case; in order to have electrons contributing to the optical conductivity one needs both to break Cooper pairs and scattering with phonons to conserve both energy and momentum. The necessity of impurities for observing the superconducting gap optically is already well-known, and becomes more evident if one plots the ratio between su-

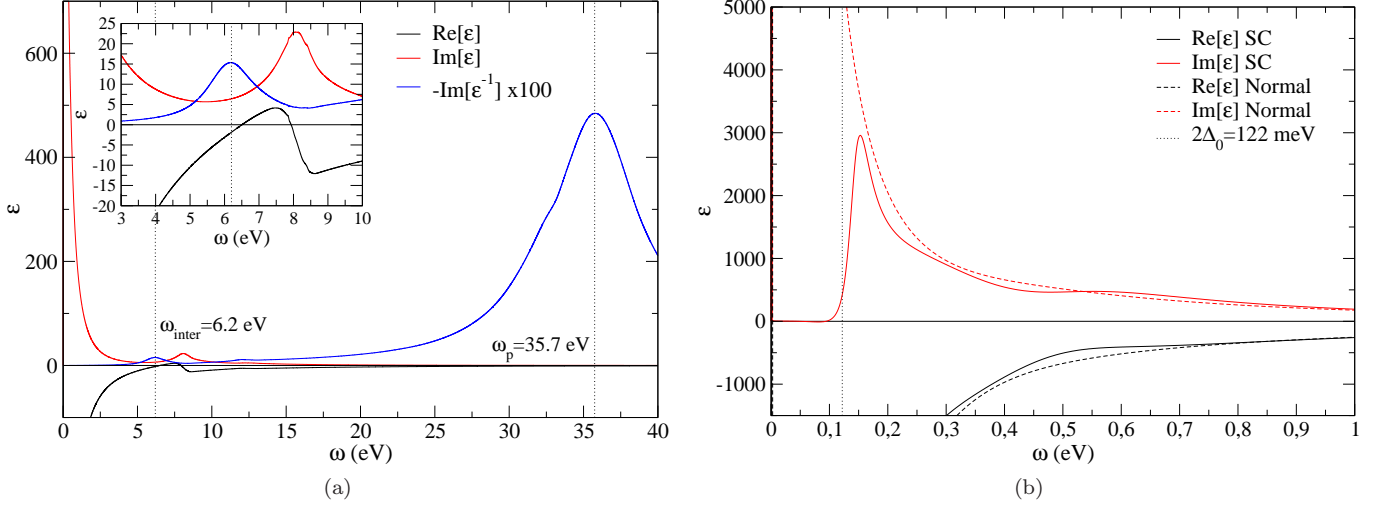


Figure 2. (a) Real and imaginary parts of the dielectric function and $-\text{Im } \epsilon^{-1}$ for $\text{I4}_1/\text{amd}$ hydrogen at 50 K and 500 GPa for $\tau_{imp}^{-1} = 200$ meV in the normal state. The inset shows the same curves zoomed in the interband plasmon region. (b) Real and imaginary parts of the dielectric function of $\text{I4}_1/\text{amd}$ hydrogen at 50 K and 500 GPa in the IR region for $\tau_{imp}^{-1} = 200$ meV in both the normal and superconducting (SC) states.

perconducting and normal state reflectance (R_{sc}/R_n) for different τ_{imp}^{-1} values (Fig. 1b). This figure clearly shows the emergence of a sharp decrease at $\hbar\omega = 2\Delta_0$ only when impurity scattering is included. The gap is observable even in the clean limit ($\tau_{imp}^{-1} = 50$ meV $< 2\Delta_0$), but the drop in R_{sc}/R_n is more notorious as one approaches the dirty limit ($\tau_{imp}^{-1} \gg 2\Delta_0$).

For photon energies larger than 1 eV the reflectivity for normal and superconducting states are almost identical (see Fig. 1a). The effect of impurity scattering up to 5 eV only yields quantitative differences keeping the shape of the reflectivity curve unaltered. In fact, for $\omega > 5$ eV all the curves both in the normal and superconducting state converge into one, suggesting electronic scattering is dominated by electronic band structure effects rather than phonons and impurities. Remarkably, in this UV regime the reflectivity sharply decreases from a high ~ 0.95 value in the visible range ($\hbar\omega = [1.6-3.3]$ eV) to ~ 0.3 at $\hbar\omega = 6.5$ eV. This stark reduction of the reflectance is a consequence of light absorption due to the presence of an interband plasmon not expected *a priori* for a simple free-electron-like alkali metal. This is demonstrated in Fig. 2a, where we display the calculated dielectric function. As revealed in the inset of this figure, the interband plasmon emerges around the energy where the real part of $\epsilon(\omega)$ vanishes and its imaginary part remains low. This induces a clear peak in $-\text{Im } \epsilon^{-1}$ at $\omega_{inter} = 6.2$ eV as shown in Fig. 2a, which coincides with the drastic drop in the reflectivity. We label this plasmon as interband because it is a consequence of the interband transitions of around 8.2 eV that occur close to the N point (see band structure in Fig. 3). Consequently, the imaginary part of the dielectric function shows a clear peak at 8.2 eV, which due to Kramers-Kronig relations makes the real

part pass through 0 at 6.5 eV and create the interband plasmon. Even if the band structure of $\text{I4}_1/\text{amd}$ is not far from the free-electron limit, the large gap opened by the electron-ion interaction at the N point⁷ suffices to induce the presence of an interband plasmon not expected for a free electron-like metal. Thus, metallic hydrogen in the $\text{I4}_1/\text{amd}$ phase is another example in which the departure from the free-electron-like character makes interband plasmons emerge and abruptly modify the optical properties, as it occurs in other simple compounds under pressure such as Li⁴⁰⁻⁴², Ca⁴³, Na^{44,45}, and AlH_3 ⁴⁶.

Apart from the interband plasmon, we find that metallic hydrogen shows the expected free-electron plasmon at $\omega_p = 35.7$ eV, which is responsible for the final decrease of the reflectivity at the extreme UV regime. This value is in good agreement with the Drude-model estimate of $\omega_p = \sqrt{4\pi N} = 35.0$ eV, where N is the total electronic density, and the 33.2 ± 3.5 eV experimental value obtained by Dias and Silvera by fitting to a Drude model only the two lowest-energy points, which are not affected by diamond absorption²⁷. This experimental fit also provided a $\tau^{-1} = 1.1 \pm 0.2$ eV estimate for the electronic scattering rate²⁷. In order to shed some light into these experimental values we fit our calculated dielectric function to a Drude model with frequency-dependent $\omega_p(\omega)$ and $\tau^{-1}(\omega)$, which are displayed in Fig. 4a (see Supplementary Material for details). In the $\hbar\omega = [0.7 - 3]$ eV range our results yield $\omega_p \sim 21$ eV and $\tau^{-1} \sim 0.6 - 1$ eV at 5 K for a clean sample, with impurities shifting τ^{-1} upwards. Our estimated τ^{-1} in the measured frequency range is in good agreement with the experiment and clearly shows that its large value is mainly due to the strong electron-phonon interaction, which highlights the fact that we are dealing with a superconductor with

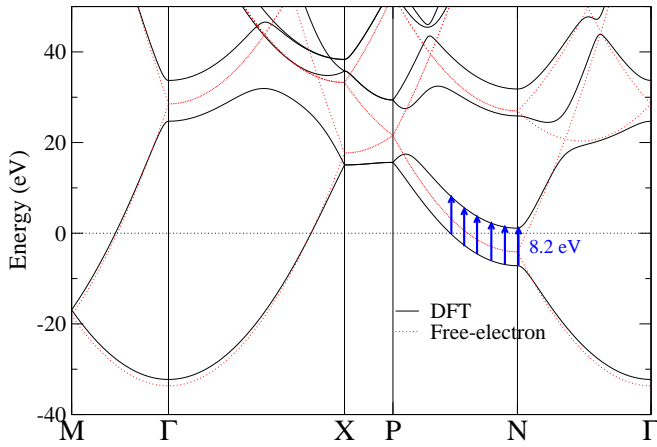


Figure 3. Electronic band-structure of I4₁/amd hydrogen at 500 GPa. Interband transitions of about 8.2 eV around the N point that yield a peak in the imaginary part of the dielectric function are marked with blue arrows. The DFT bands are compared to the free-electron band structure. The Fermi level is at 0 eV.

a very large T_c . Indeed, the electron-electron scattering contribution to τ^{-1} is negligible in this frequency range as shown by the pure TDDFT calculation. The value obtained for ω_p is considerably lower than the one obtained by Silvera and Dias^{22,27}, but it is consistent with the $\omega_p^{intra} = \sqrt{4\pi N_{intra}} = 22.6$ eV value, where N_{intra} is the electronic density contributing to intraband transitions (see Supplementary Material for details). Nonetheless, in this low energy ($\omega \ll \omega_p$) regime very different ω_p values still provide a good fitting to the experimental data, while τ^{-1} remains almost unaltered (see Supplementary Material). We thus consider the τ^{-1} value obtained experimentally^{22,27} to be more meaningful than the plasma frequency, because indeed it is this parameter what determines how much the reflectivity deviates from one for $\omega \ll \omega_p$.

In Fig. 4b we show how the raw experimental values in Ref. [22] compare to our calculations at 5 and 83 K, with reflectivity calculated for a hydrogen/diamond interface by using the refractive index of $n = 2.41$ of diamond instead of $n = 1$ in eq. 1. Our results compare well at 5 K to the two lowest frequency experimental data points, which are the ones considered for fitting ω_p and τ^{-1} with the Drude model as the other points might have been affected by absorption of light by diamond^{22,27}. The sharp offset of reflectivity due to the superconducting gap lays off the IR absorption range of diamond, and should be measurable in consequence. UV absorption of diamond however would eclipse the minimum of the reflectivity predicted here at 6.5 eV due to the presence of the interband plasmon, since above the indirect electronic bandgap of 5.47 eV (at zero pressure) diamond is no longer transparent. In any case, the sharp decrease associated to such plasmon starts before the absorption onset and should be observable in pure diamond. Interestingly, recent studies

claim the diamond bandgap increases with pressure⁴⁷, which would make the reflectivity drop induced by the interband plasmon easier to observe. However, impurities in diamond could be responsible of light absorption at lower energies, even in the visible²⁷. In order to disentangle whether the reflectivity drop observed experimentally is a consequence of diamond absorption or reflects the presence of the intraband plasmon we are predicting here, a proper characterization of the optical properties of diamond at the experimental conditions is required.

Regarding the temperature dependence of the reflectivity observed in the experiment, according to our calculations temperature only affects the region within some meVs around the superconducting gap. In the experimental region our calculations are practically temperature independent, as it can be seen for both reflectivity and scattering rate values (see Fig. 4). This indicates the temperature dependence of reflectivity shown in the experiments cannot be explained with the increase of phonon occupation in the system. Motivated by uncertainties in the reported pressure of the experiment^{23–26}, we have also calculated the optical spectra for I4₁/amd hydrogen at 400 and 600 GPa and only found minor quantitative differences with respect to the 500 GPa results analyzed in detail here, so that the analysis holds. The energy of the interband plasmon at 400 GPa is 5.5 eV and 6.6 eV at 600 GPa (more details on the Supplementary Material).

In conclusion, we have made an exhaustive analysis of the optical response properties of I4₁/amd metallic hydrogen from the infrared to the extreme ultraviolet. Our results show that in the measured energy range²² the electronic scattering is dominated by the huge electron-phonon interaction of the system. Besides, our calculations reveal a sharp onset of the optical conductivity in the infrared region induced by the very large superconducting gap and a pronounced loss of reflectance in the ultraviolet regime due to the presence of a non-free-electron-like interband plasmon. Thus, our work deeply encourages further experimental research in order to extend optical measurements both to the ultraviolet and infrared. Confirming the predicted interband plasmon and measuring the superconducting gap optically would be not only of tremendous interest by itself, but also a big step towards characterizing this fascinating material.

The authors acknowledge financial support from the Spanish Ministry of Economy and Competitiveness (FIS2016-76617-P) and the Department of Education, Universities and Research of the Basque Government and the University of the Basque Country (IT756-13). M.B. is also thankful to the Department of Education, Language Policy and Culture of the Basque Government for a predoctoral fellowship (Grant No. PRE-2015-2-0269). Computer facilities were provided by the Donostia International Physics Center (DIPC). JIA acknowledges the Impuls und Vernetzungsfonds der Helmholtz-Gemeinschaft Postdoc Programme.

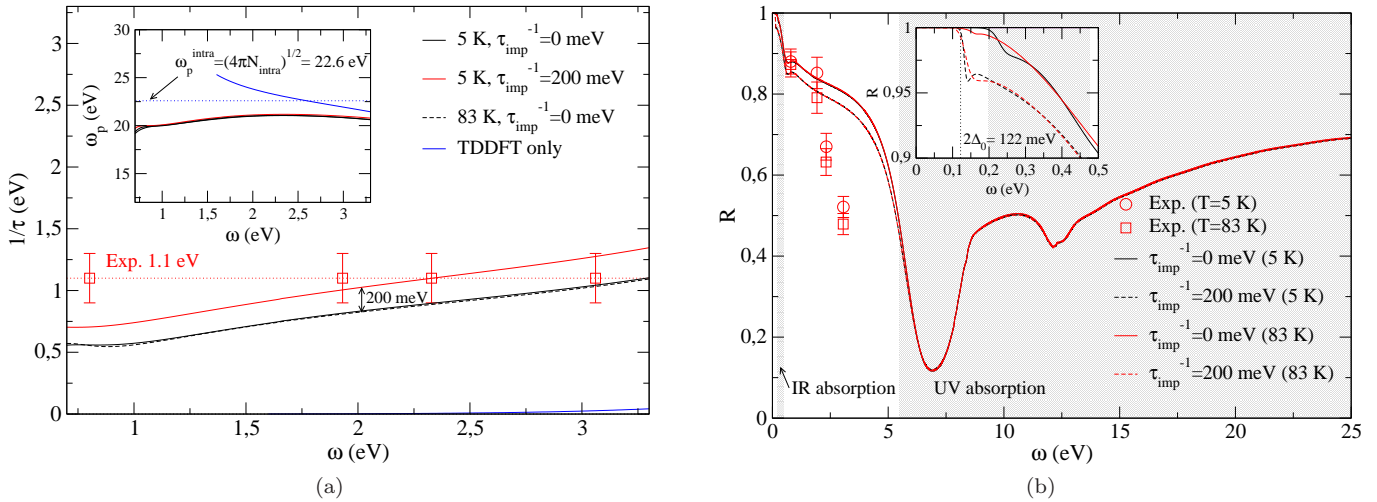


Figure 4. (a) Frequency-dependent electronic scattering rate of I41/amd hydrogen at 500 GPa for different impurity scattering rates and temperatures in the region in which the experiments in Ref. [22] were performed. The same curve is also obtained for the case in which the ME formalism is not considered. The experimental $\tau^{-1} = 1.1 \pm 0.2$ eV estimate is also included²⁷. The inset shows the obtained frequency dependent $\omega_p(\omega)$ in the same energy range, together with the ω_p^{intra} estimate. (b) Reflectivity of a I41/amd hydrogen/diamond interface at 5 and 83 K at 500 GPa for different impurity scattering rates. Diamond IR (0.2-0.47 eV) and UV (5.47 eV electronic bandgap) absorption regions are shown in shaded gray. Experimental raw values²² are included.

- ¹ E. Wigner and H. B. Huntington, *The Journal of Chemical Physics* **3**, 764 (1935).
- ² N. W. Ashcroft, *Phys. Rev. Lett.* **21**, 1748 (1968).
- ³ P. Cudazzo, G. Profeta, A. Sanna, A. Floris, A. Continenza, S. Massidda, and E. K. U. Gross, *Phys. Rev. Lett.* **100**, 257001 (2008).
- ⁴ J. M. McMahon and D. M. Ceperley, *Phys. Rev. B* **84**, 144515 (2011).
- ⁵ Y. Yan, J. Gong, and Y. Liu, *Physics Letters A* **375**, 1264 (2011).
- ⁶ E. Maksimov and D. Savrasov, *Solid State Communications* **119**, 569 (2001).
- ⁷ M. Borinaga, I. Errea, M. Calandra, F. Mauri, and A. Bergara, *Phys. Rev. B* **93**, 174308 (2016).
- ⁸ M. Borinaga, P. Riego, A. Leonardo, M. Calandra, F. Mauri, A. Bergara, and I. Errea, *Journal of Physics: Condensed Matter* **28**, 494001 (2016).
- ⁹ I. F. Silvera and J. W. Cole, *Journal of Physics: Conference Series* **215**, 012194 (2010).
- ¹⁰ M. I. Erements and I. A. Troyan, *Nat Mater* **10**, 927 (2011).
- ¹¹ P. Loubeyre, R. LeToullec, D. Hausermann, M. Hanfland, R. J. Hemley, H. K. Mao, and L. W. Finger, *Nature* **383**, 702 (1996).
- ¹² S. Deemyad and I. F. Silvera, *Phys. Rev. Lett.* **100**, 155701 (2008).
- ¹³ A. B. Stanimir, E. Schwegler, T. Ogitsu, and G. Galli, *Nature* **431**, 669 (2004).
- ¹⁴ H.-k. Mao and R. J. Hemley, *Rev. Mod. Phys.* **66**, 671 (1994).
- ¹⁵ C.-S. Zha, Z. Liu, and R. J. Hemley, *Phys. Rev. Lett.* **108**, 146402 (2012).
- ¹⁶ A. F. Goncharov, E. Gregoryanz, R. J. Hemley, and H.-k. Mao, *Proceedings of the National Academy of Sciences* **98**, 14234 (2001).
- ¹⁷ R. T. Howie, C. L. Guillaume, T. Scheler, A. F. Goncharov, and E. Gregoryanz, *Phys. Rev. Lett.* **108**, 125501 (2012).
- ¹⁸ C.-s. Zha, Z. Liu, M. Ahart, R. Boehler, and R. J. Hemley, *Phys. Rev. Lett.* **110**, 217402 (2013).
- ¹⁹ R. T. Howie, P. Dalladay-Simpson, and E. Gregoryanz, *Nat Mater* **14**, 495 (2015).
- ²⁰ P. Loubeyre, F. Occelli, and R. LeToullec, *Nature* **416**, 613 (2002).
- ²¹ P. Dalladay-Simpson, R. T. Howie, and E. Gregoryanz, *Nature* **529**, 63 (2016).
- ²² R. P. Dias and I. F. Silvera, *Science* **355**, 715 (2017).
- ²³ M. I. Erements and A. P. Drozdov, (2017), [arXiv:1702.05125](https://arxiv.org/abs/1702.05125).
- ²⁴ P. Loubeyre, F. Occelli, and P. Dumas, (2017), [arXiv:1702.07192](https://arxiv.org/abs/1702.07192).
- ²⁵ X.-D. Liu, P. Dalladay-Simpson, R. T. Howie, B. Li, and E. Gregoryanz, (2017), [arXiv:1704.07601](https://arxiv.org/abs/1704.07601).
- ²⁶ A. F. Goncharov and V. V. Struzhkin, (2017), [arXiv:1702.04246](https://arxiv.org/abs/1702.04246).
- ²⁷ I. Silvera and R. Dias, (2017), [arXiv:1704.03064](https://arxiv.org/abs/1704.03064).
- ²⁸ M. I. Erements, I. A. Troyan, and A. P. Drozdov, (2016), [arXiv:1601.04479](https://arxiv.org/abs/1601.04479).
- ²⁹ C. J. Pickard and R. J. Needs, *Nat Phys* **3**, 473 (2007).
- ³⁰ A. Perucchi, L. Baldassarre, P. Postorino, and S. Lupi, *Journal of Physics: Condensed Matter* **21**, 323202 (2009).
- ³¹ S. Azadi, B. Monserrat, W. M. C. Foulkes, and R. J. Needs, *Phys. Rev. Lett.* **112**, 165501 (2014).
- ³² J. M. McMahon and D. M. Ceperley, *Phys. Rev. Lett.* **106**, 165302 (2011).
- ³³ Z. Schlesinger, R. T. Collins, D. L. Kaiser, and

- F. Holtzberg, [Phys. Rev. Lett. **59**, 1958 \(1987\)](#).
- ³⁴ L. D. Rotter, Z. Schlesinger, J. P. McCauley, N. Coustel, J. E. Fischer, and A. B. Smith, [Nature **355**, 532 \(1992\)](#).
- ³⁵ A. P. Drozdov, M. I. Erements, I. A. Troyan, V. Ksenofontov, and S. I. Shylin, [Nature **525**, 73 \(2015\)](#).
- ³⁶ F. Capitani, B. Langerome, J.-B. Brubach, P. Roy, A. Drozdov, M. I. Erements, E. J. Nicol, J. P. Carbotte, and T. Timusk, [Nat Phys advance online publication \(2017\)](#), article.
- ³⁷ E. Runge and E. K. U. Gross, [Phys. Rev. Lett. **52**, 997 \(1984\)](#).
- ³⁸ M. Petersilka, U. J. Gossmann, and E. K. U. Gross, [Phys. Rev. Lett. **76**, 1212 \(1996\)](#).
- ³⁹ B. Rousseau, A. Eiguren, and A. Bergara, [Phys. Rev. B **85**, 054305 \(2012\)](#).
- ⁴⁰ V. M. Silkin, A. Rodriguez-Prieto, A. Bergara, E. V. Chulkov, and P. M. Echenique, [Phys. Rev. B **75**, 172102 \(2007\)](#).
- ⁴¹ A. Rodriguez-Prieto, V. M. Silkin, A. Bergara, and P. M. Echenique, [New J. Phys. **10**, 053035 \(2008\)](#).
- ⁴² I. Errea, A. Rodriguez-Prieto, B. Rousseau, V. M. Silkin, and A. Bergara, [Phys. Rev. B **81**, 205105 \(2010\)](#).
- ⁴³ I. Errea, B. Rousseau, A. Eiguren, and A. Bergara, [Phys. Rev. B **86**, 085106 \(2012\)](#).
- ⁴⁴ J. Ibañez Azpiroz, B. Rousseau, A. Eiguren, and A. Bergara, [Phys. Rev. B **89**, 085102 \(2014\)](#).
- ⁴⁵ H.-K. Mao, Y. Ding, Y. Xiao, P. Chow, J. Shu, S. Lebgue, A. Lazicki, and R. Ahuja, [Proc. Natl. Acad. Sci. USA **108**, 20434 \(2011\)](#).
- ⁴⁶ I. G. Gurtubay, B. Rousseau, and A. Bergara, [Phys. Rev. B **82**, 085113 \(2010\)](#).
- ⁴⁷ E. J. Gamboa, L. B. Fletcher, H. J. Lee, M. J. Macdonald, U. Zastrau, M. Gauthier, D. Gericke, J. Vorberger, E. Granados, J. B. Hastings, and S. H. Glenzer, [unpublished \(2016\)](#).

Supplementary Material

Strong electron-phonon and band structure effects in the optical properties of high pressure metallic hydrogen

Miguel Borinaga^{1,2}, Julen Ibañez-Azpiroz³, Aitor Bergara^{1,2,4} and Ion Errea^{2,5}

¹*Centro de Física de Materiales CFM, CSIC-UPV/EHU, Paseo Manuel de Lardizabal 5, 20018 Donostia/San Sebastián, Basque Country, Spain*

²*Donostia International Physics Center (DIPC), Manuel Lardizabal pasealekua 4, 20018 Donostia/San Sebastián, Basque Country, Spain*

³*Peter Grünberg Institute and Institute for Advanced Simulation, Forschungszentrum Jülich & JARA, D-52425 Jülich, Germany*

⁴*Departamento de Física de la Materia Condensada, University of the Basque Country (UPV/EHU), 48080 Bilbao, Basque Country, Spain*

⁵*Fisika Aplikatua 1 Saila, Bilboko Ingeniaritza Eskola, University of the Basque Country (UPV/EHU), Rafael Moreno "Pitxitxi" Pasealekua 3, 48013 Bilbao, Basque Country, Spain*

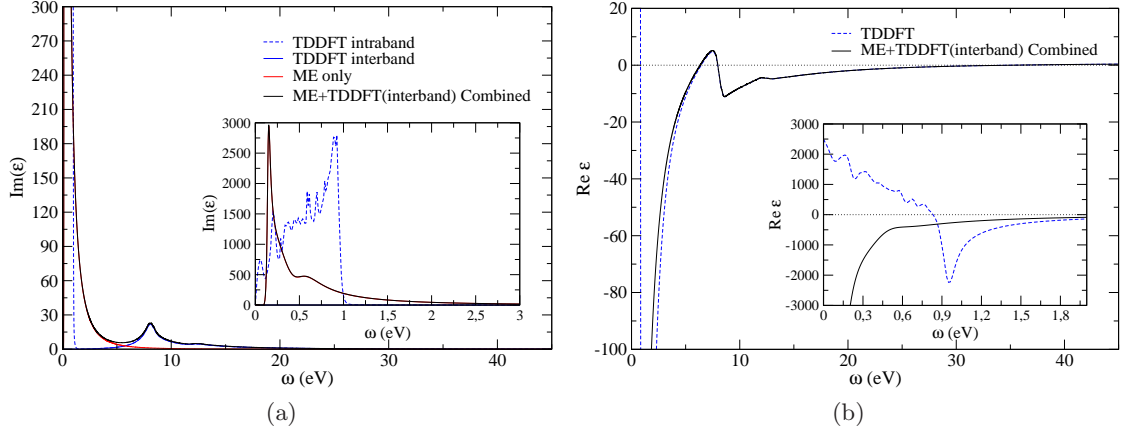


Figure 1: (a) Different contributions to the imaginary part of ε of $\text{I4}_1/\text{amd}$ hydrogen at 500 GPa. The inset shows a zoom into lower energies. (b) Real part of ε calculated using the Kramers-Kronig relations.

1 Calculation methods and procedure

The central quantity addressed in this work is the frequency dependent reflectivity, which for normal incident light in a medium with refractive index n can be written as

$$R(\omega) = \left| \frac{\sqrt{\varepsilon(\omega)} - n}{\sqrt{\varepsilon(\omega)} + n} \right|^2, \quad (1)$$

where the relative dielectric function $\varepsilon(\omega)$ can be expressed in terms of the optical conductivity $\sigma(\omega)$ as

$$\varepsilon(\omega) = 1 + i \frac{4\pi\sigma(\omega)}{\omega}. \quad (2)$$

The optical conductivity of a metal can be described as

$$\sigma(\omega) = \sigma_{intra}(\omega) + \sigma_{inter}(\omega) + \sigma_{phonons}(\omega), \quad (3)$$

where σ_{intra} and σ_{inter} account, respectively, for the optical conductivity provided by electronic intraband and interband transitions, while $\sigma_{phonons}$ accounts for the direct phonon absorption contribution. As $\text{I4}_1/\text{amd}$ hydrogen lacks of IR active vibrational modes [1], we set $\sigma_{phonons} = 0$.

The interband and intraband contributions are computed in two stages. We first calculate the dielectric function within time-dependent DFT [2, 3] (TDDFT), which realistically incorporates the actual electronic structure into the dielectric function. The dielectric function is calculated by employing an interpolation scheme [4–6] of both the Kohn-Sham states and the matrix elements with the use of maximally localized Wannier functions [7, 8]. The method allows a very fine sampling of the reciprocal space. In order to avoid numerical problems, a finite but small momentum is taken for the calculation of

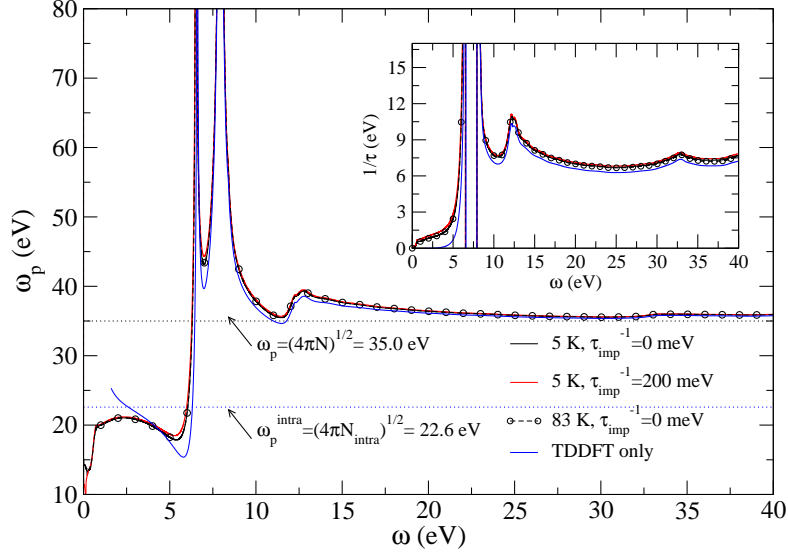


Figure 2: Drude model frequency-dependent plasma frequency $\omega_p(\omega)$ of I41/amd hydrogen at 500 GPa for different impurity scattering rates and temperatures. The same curve is also obtained for the case in which the ME formalism is not considered (TDDFT only). The inset shows the frequency-dependent impurity scattering rate $\tau^{-1}(\omega)$.

the dielectric function. The obtained optical conductivity from the TDDFT calculation thus contains both interband and intraband contributions: $\sigma^{TDDFT}(\omega) = \sigma_{intra}^{TDDFT}(\omega) + \sigma_{inter}^{TDDFT}(\omega)$. In order to incorporate the fine features of the band structure, we set $\sigma_{inter}(\omega) = \sigma_{inter}^{TDDFT}(\omega)$ in Eq. (3), which provides a fine description of the reflectivity at high energies. The low-energy intraband contribution given by $\sigma_{intra}^{TDDFT}(\omega)$ is affected by the choice of a finite momentum and completely neglects how an excited electron can decay due to the electron-phonon interaction. Moreover, this regime can also be strongly affected in superconductors due to the presence of the superconducting gap [9–11]. In order to incorporate these effects into the reflectivity, the intraband contribution to the optical conductivity is calculated instead by solving the isotropic Migdal-Eliashberg (ME) equations. We thus make $\sigma_{intra}(\omega) = \sigma^{ME}(\omega)$, where $\sigma^{ME}(\omega)$ is the optical conductivity obtained solving ME equations. Following Ref. [12], these equations are solved in the imaginary axis using a Padé approximant for the analytic continuation to the real frequency axis. The free-electron density used in the ME equations is determined so that the partial f-sum rule integral

$$\int_0^\infty \text{Re } \sigma^{ME}(\omega) d\omega = \int_0^\infty \text{Re } \sigma_{intra}^{TDDFT}(\omega) d\omega \quad (4)$$

is satisfied by $\sigma^{ME}(\omega)$. This guarantees that the total optical conductivity in Eq. (3) satisfies the f-sum rule and yields the correct electron density. This procedure can be performed because the interband and intraband contributions in the TDDFT optical conductivities (real part) are clearly separated as it can be seen in Fig. 1a for $\text{Im } \epsilon(\omega) = \omega \text{Re } \sigma(\omega)/4\pi$. The real part of ϵ (Fig. 1b) is obtained afterwards using the Kramers-

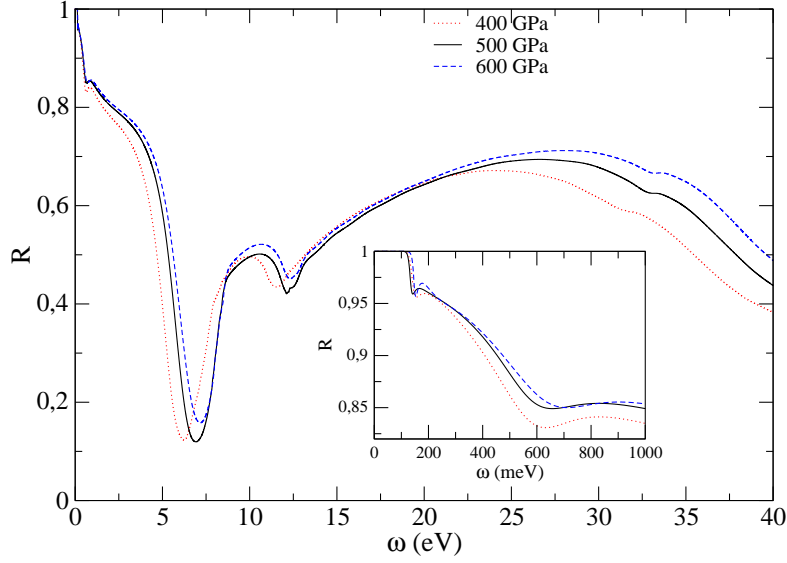


Figure 3: Reflectivity of a $I4_1/amd$ hydrogen/diamond interface at 400, 500 and 600 GPa at 5 K and $\tau_{imp}^{-1} = 200$ meV in the superconducting state.

Kronig relations. Performing the f-sum rule integral (Eq. (4)) for each contribution in the TDDFT calculation we obtain $\omega_p^{intra} = \sqrt{4\pi N_{intra}} = 22.6$ eV and $\omega_p^{inter} = \sqrt{4\pi N_{inter}} = 26.3$ eV, with $\omega_p = \sqrt{4\pi N} = \sqrt{4\pi(N_{intra} + N_{inter})} = 35.0$ eV, with N_{intra} and N_{inter} being the electronic density contributing to the intraband and interband processes respectively.

All ground state DFT calculations are performed at 400, 500 and 600 GPa, where metallic hydrogen is predicted to adopt the $I4_1/amd$ crystal structure [13, 14]. We employ the QUANTUM-ESPRESSO package [15], using a plane-wave energy cutoff of 100 Ry and an ultrasoft pseudopotential [16] with the Perdew-Wang parametrization of the local-density-approximation [17] for the exchange and correlation potential. The wannierization process includes the 40 lowest-lying bands and is performed using the WANNIER90 package [18]. It allows us to interpolate the original $20 \times 20 \times 20$ \mathbf{k} -space mesh into a fine $60 \times 60 \times 60$ mesh for the calculation of the TDDFT dielectric function. In the latter crystal local field effects are taken into account by the use of two reciprocal lattice shells [4, 6]. The Eliashberg function $\alpha^2 F(\omega)$ function needed to solve the ME equations is calculated as described in Ref. [1], but with the use of the same exchange and correlation potential as for the TDDFT calculation. $\alpha^2 F(\omega)$ is calculated at the harmonic level as anharmonicity barely affects it [1]. ME equations were solved using a Matsubara energy cutoff of 6 times the highest phonon frequency, and the same as for computing the Padé approximant. We solved the ME equations assuming different τ_{imp}^{-1} impurity scattering rates as the latter is introduced as a parameter in the equations.

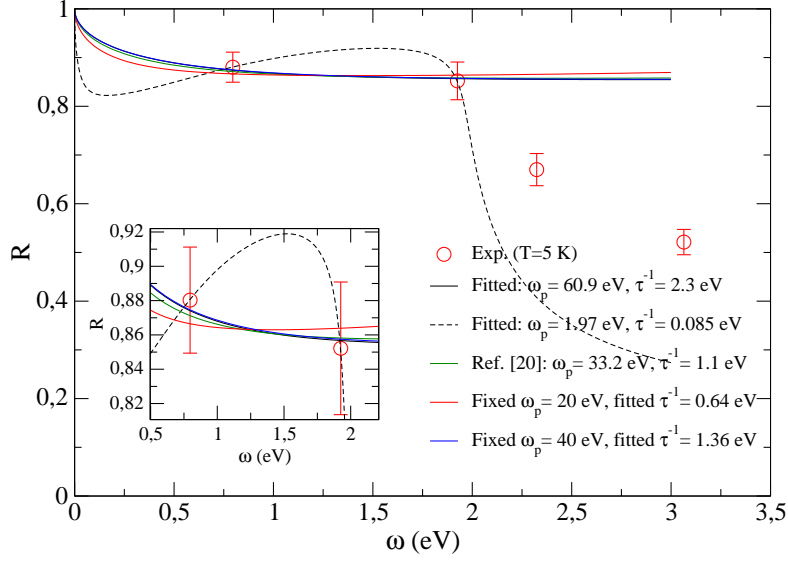


Figure 4: Experimental data at 5 K [19] fitted with the Drude model (only the two lowest energy data points are fitted). Solid and dashed black curves show our two different fitting results, while the green curve shows the fitting by Dias *et al.*[20]. Red and blue curves show the curves obtained by fitting only τ^{-1} for ω_p fixed at 20 and 40 eV respectively.

2 Drude model

In Ref. [19] the authors fitted the experimental data with the reflectivity formula following the Drude model. According to this model,

$$\varepsilon(\omega) = 1 - \frac{\omega_p^2 \tau}{\omega} \frac{1}{i + \omega \tau}. \quad (5)$$

While often the plasma frequency ω_p and the mean scattering time τ are defined as fixed parameters, it can also be useful to generalize this formula by making them frequency dependent. This way, for a known $\varepsilon(\omega)$, one can define $\omega_p(\omega)$ and $\tau(\omega)$ as

$$\frac{1}{\tau(\omega)} = \frac{\omega \text{Im } \varepsilon(\omega)}{1 - \text{Re } \varepsilon(\omega)} \quad (6)$$

$$\omega_p^2(\omega) = \omega \tau(\omega) \left(\omega^2 + \frac{1}{\tau(\omega)^2} \right) \text{Im } \varepsilon(\omega). \quad (7)$$

We have calculated $\tau^{-1}(\omega)$ and $\omega_p(\omega) \equiv +\sqrt{|\omega_p^2(\omega)|}$ using $\varepsilon(\omega)$ values calculated for different impurity scattering rates and temperatures, as well as only considering TDDFT and therefore neglecting phonon and impurity scattering. In Fig. 2 we can see that for frequencies larger than 15 eV, all ω_p curves converge in a plateau close to the theoretical $\omega_p = \sqrt{4\pi N} = 35.0$ eV value, while τ^{-1} yields around 7 eV, regardless of whether or not including phonon and impurity scattering. This shows electronic scattering is dominated

Pressure (GPa)	400	500	600
Δ_0 (meV)	64.1	61.0	67.1
ω_0 (eV)	7.6	8.2	8.2
ω_{inter} (eV)	5.5	6.5	6.6
ω_p (eV)	34.2	35.7	36.8

Table 1: Superconducting electronic bandgap (Δ_0), interband absorption peak position (ω_0), interband plasmon peak position (ω_{inter}) and total plasma frequency (ω_p) of I4₁/amd hydrogen at different pressures.

by electronic band structure effects in this high frequency regime. For frequencies lower than 5 eV but larger than 0.5 eV approximately, ω_p yields values around 21 eV, close to the $\omega_p = \sqrt{4\pi N_{intra}} = 22.6$ eV value, which is expected as the interband transitions occur at higher energies and therefore their corresponding electronic density does not contribute to ε . In this low energy regime, τ^{-1} ranges 0.7-1.5 eV when phonon and impurity scattering is included in the calculation even if for the TDDFT only calculation yields negligible values. This shows phonon and impurities clearly govern electronic scattering for the photon energies the experiment was performed at. In the 5-15 eV interband plasmon region, ω_p and τ^{-1} take unrealistic (even negative for τ^{-1}) values. This is because the Drude formula is not adequate for modeling the optical conductivity close to interband excitations. In order to take into account the interband transitions and their contribution to ε , one should add a Lorentz Oscillator. The same holds for the very small energy region ($\omega < 0.5$ eV), as the ω dependence of the electron-phonon and impurity scattering contribution to ε is more complex than the one modeled by the Drude formula.

3 Fitting of experimental data

In Ref. [19] the authors fitted four experimental data points for each temperature (5 and 83 K), where reflectivity was corrected for taking into account diamond absorption. However, later they claimed this correction procedure may not be valid and thus only considered the lowest two energy raw (not corrected) data points[20], obtaining similar values for ω_p and τ^{-1} at 5 K. However, fitting a non-linear formula consisting of two parameters to only two experimental points results in a non-unique solution for the fitting parameters. By fitting the first two experimental data points at 5 K to the reflectivity formula we have obtained at least two different results: $\omega_p = 60.91$ eV and 1.98 eV and with $\tau^{-1} = 2.21$ eV and 0.085 eV respectively (see Fig. 4). None of the fitted ω_p values are reasonable, either for too high or too low. It is also important to notice we do not obtain the same fitting parameters as in Ref. [20] ($\omega_p = 33.2$ eV and $\tau^{-1} = 1.1$ eV). However, if we set $\omega_p = 33.2$ eV and fit only τ^{-1} we obtain the same 1.1 eV as in Ref. [20]. We have seen that for ω_p values fixed within 20-40 eV (values close to what is expected for a nearly-free-electron-like metal at these densities) and fitted only τ^{-1} to the experimental data, the latter only oscillates within 0.64-1.36 eV yielding a good fitting to the experiments within the error bars.

4 Pressure dependence

Due to the doubts on the pressure calibration [21–24] in Ref. [19] we have calculated the reflectivity of a $\text{I4}_1/\text{amd}$ hydrogen/diamond interface at 400 and 600 GPa as well at 5 K and $\tau_{imp}^{-1} = 200$ meV in the superconducting state. As we can see in Fig. 3, differences are only quantitative, as the qualitative nature of the curves does not change. The minor quantitative changes of the main parameters are summarized in Table 1.

References

- [1] M. Borinaga, I. Errea, M. Calandra, F. Mauri, and A. Bergara, *Phys. Rev. B* **93**, 174308 (2016).
- [2] E. Runge and E. K. U. Gross, *Phys. Rev. Lett.* **52**, 997 (1984).
- [3] M. Petersilka, U. J. Gossmann, and E. K. U. Gross, *Phys. Rev. Lett.* **76**, 1212 (1996).
- [4] B. Rousseau, A. Eiguren, and A. Bergara, *Phys. Rev. B* **85**, 054305 (2012).
- [5] I. Errea, B. Rousseau, A. Eiguren, and A. Bergara, *Phys. Rev. B* **86**, 085106 (2012).
- [6] J. Ibañez Azpiroz, B. Rousseau, A. Eiguren, and A. Bergara, *Phys. Rev. B* **89**, 085102 (2014).
- [7] N. Marzari and D. Vanderbilt, *Phys. Rev. B* **56**, 12847 (1997).
- [8] N. Marzari, A. A. Mostofi, J. R. Yates, I. Souza, and D. Vanderbilt, *Rev. Mod. Phys.* **84**, 1419 (2012).
- [9] Z. Schlesinger, R. T. Collins, D. L. Kaiser, and F. Holtzberg, *Phys. Rev. Lett.* **59**, 1958 (1987).
- [10] L. D. Rotter, Z. Schlesinger, J. P. McCauley, N. Coustel, J. E. Fischer, and A. B. Smith, *Nature* **355**, 532 (1992).
- [11] F. Capitani, B. Langerome, J. B. Brubach, P. Roy, A. Drozdov, M. I. Erements, E. J. Nicol, J. P. Carbotte, and T. Timusk, (2016), [arXiv:1612.06732](#).
- [12] N. E. Bickers, D. J. Scalapino, R. T. Collins, and Z. Schlesinger, *Phys. Rev. B* **42**, 67 (1990).
- [13] S. Azadi, B. Monserrat, W. M. C. Foulkes, and R. J. Needs, *Phys. Rev. Lett.* **112**, 165501 (2014).
- [14] J. M. McMahon and D. M. Ceperley, *Phys. Rev. Lett.* **106**, 165302 (2011).

- [15] P. Giannozzi *et al.*, [J. Phys. Condens. Matter](#) **21**, 395502 (2009).
- [16] D. Vanderbilt, [Phys. Rev. B](#) **41**, 7892 (1990).
- [17] J. P. Perdew and Y. Wang, [Phys. Rev. B](#) **45**, 13244 (1992).
- [18] A. A. Mostofi, J. R. Yates, G. Pizzi, Y.-S. Lee, I. Souza, D. Vanderbilt, and N. Marzari, [Computer Physics Communications](#) **185**, 2309 (2014).
- [19] R. P. Dias and I. F. Silvera, [Science](#) **355**, 715 (2017).
- [20] I. Silvera and R. Dias, (2017), [arXiv:1704.03064](#) .
- [21] M. I. Eremets and A. P. Drozdov, (2017), [arXiv:1702.05125](#) .
- [22] P. Loubeyre, F. Occelli, and P. Dumas, (2017), [arXiv:1702.07192](#) .
- [23] X.-D. Liu, P. Dalladay-Simpson, R. T. Howie, B. Li, and E. Gregoryanz, (2017), [arXiv:1704.07601](#) .
- [24] A. F. Goncharov and V. V. Struzhkin, (2017), [arXiv:1702.04246](#) .